butions.

[6]M. Foster and C. Quigg, Phys. Rev. D **7**, 108 (1973).

[7]J. Ellis, J. Finkelstein, and R. D. Peccei, Nuovo Cimento **12B**, 763 (1972).

[8]R. Blankenbecler and T. L. Neff, Phys. Rev. D **5**, 128 (1972).

[9]G. Goldhaber, S. Goldhaber, W. Lee, and A. Pais, Phys. Rev. **120**, 300 (1960).

Muon-Nucleon Inelastic Interactions at High Energy

P. L. Jain, R. D. Malucci, M. J. Potoczak, and N. J. Wixon*

High Energy Experimental Laboratory, Department of Physics, State University of New York at Buffalo, Buffalo, New York 14214

(Received 21 August 1972)

The inelastic interactions of 10.1-GeV/c positive and 15.8-GeV/c negative muons produced at the Brookhaven alternating gradient synchrotron have been studied in nuclear emulsions. Secondary particles produced in these interactions have been identified; their energy spectrum and angular distribution (in the c.m. system) are given for pions, kaons, and protons along with their partial cross sections. The inclusive pion-production reaction is studied and the relative shapes of the P_t^2 (squared transverse momentum) and p_l (longitudinal momentum) distributions are discussed and compared with γp, πp, and pp reactions. The partial and integral cross sections have been measured for both beams along with the energy dependence of their total cross sections and are compared with theory by using the first, second, and fourth powers of $1/(1 + q^2/m_\rho^2)$ for $\sigma_{\exp}(q^2, \nu)$, the quantity commonly called the "virtual-photon–nucleon total cross section." The values of the structural function νW_2 are calculated for $0.025 \leqslant q^2 \leqslant 0.3$ (GeV/c)^2 and large values of $\omega' \geqslant 10$. The present data are compared with the previous muon data of Perl at low q^2 values, and various theoretical models are considered to test scaling at low q^2 values.

I. INTRODUCTION

Inelastic lepton-nucleon scattering at high energies has been carried out at various accelerators for over a decade. The higher energies and intensities have made available a new region of inelastic scattering commonly referred to as the "deep-inelastic" region, which corresponds to the excitation of the continuum well beyond the resonance region. One of the most interesting results emerging from these high–momentum-transfer studies is the possibility of obtaining detailed information about the small-distance nucleon structure and any fundamental constituents of hadrons. But before we can explain these data, we need to have a detailed understanding of strong interactions, which is not yet entirely available. Since the first theoretical predictions by Bjorken[1] and the experimental discovery[2] of "scaling" in electron-proton scattering there have been substantial theoretical attempts to understand this phenomena through the applications of Regge theory,[3] vector-meson dominance,[4] parton theory,[5] duality,[6] and space-time phenomenology of photon absorption.[7]

In strong-interaction physics, most of the progress has depended upon experiments in which most or all of the particles from a particular

event were detected. Similarly we expect that progress in electroproduction and muon production will depend a great deal on such experiments. But in electroproduction, the radiative energy loss of the electron gives rise to a large background of real photons near the inelastic scattering target and thus cause some difficulties in completely detecting all the particles emitted. Almost all the existing data from electron-nucleon scattering have been obtained at fixed outgoing angles[2,8] while ignoring the final hadronic state. Muons, on the other hand, because of the smaller electromagnetic background and radiation corrections (resulting from the larger mass of the muon) may be a better probe than electrons for exploring some aspects of particle physics.

Most high-energy work in lepton-nucleon inelastic scattering has been done at large q^2 [$\geqslant 1$ (GeV/c)^2] with the use of electron beams, and this range is where scaling has been observed. However what happens at low q^2 is a question that has not yet been answered. Also, owing to the two-component picture of photons, i.e., suri and Yennie's[5] short- and long-range interactions of photons with nucleons, one may also check the hadronic interaction of the physical photon for low-q^2 lepton-nucleon collisions which so far has not been presented. For small-q^2 events, one could

also check Yang's hypothesis of fragmentation of the target nucleon.[9] Thus, in the present experimental research work with 10.1- and 15.8-GeV/c positive and negative muon-nucleon inelastic interactions we are interested in the following general aspects of muon-nucleon inelastic interactions:

(i) the interactions at small angles and at relatively low q^2 values,

(ii) the scaling at low q^2 values,

(iii) the production of secondary particles in muon-nucleon interactions,

(iv) Yang's hypothesis of limiting fragmentations for the target nucleon by the muon projectile,

(v) the electromagnetic equivalence of muon and electron at these energies,

(vi) our muon-nucleon data for inelastic interactions compared with the other muon-nucleon available data, and

(vii) the question of which of the theoretical models mentioned earlier will best represent our data.

II. KINEMATICS AND DYNAMICS

The general interaction $\mu + N \rightarrow \mu + $ anything is kinematically simple if one detects only the scattered muon. Figure 1 shows a muon of four-momentum $p = (E, \vec{p})$ scattering off a nucleon of four-momentum $P = (M, \vec{0})$ and producing the final leptonic and hadronic states of $p' = (E, \vec{p}')$ and $P' = (M + \nu, \vec{q})$, respectively. The collision is thought to occur via the exchange of a photon (of four-momentum q); q^2 stands for the (mass)^2 of the photon with ν the laboratory energy transfer, and M the mass of the nucleon. Since we know the interaction at the muon-photon vertex and the photon propagator, we may factor out these contributions and study what is happening at the other vertex. If we do not observe the details of the final hadronic state, then everything must be a function of just the two variables

$$q^2 = -(p - p')^2$$
$$= 4EE' \sin^2(\tfrac{1}{2}\theta) \tag{1}$$
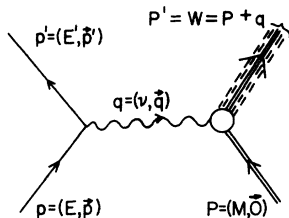

FIG. 1. One-photon exchange diagram for muon-nucleon inelastic scattering.

and

$$\nu = q_0$$
$$= (\vec{p} \cdot \vec{q})/M$$
$$= E - E', \tag{2}$$

while θ being the scattered angle of the muon. The invariant mass W of the final hadronic state, called the missing mass, is related to ν and q^2 by

$$W^2 = s$$
$$= (P + q)^2$$
$$= M^2 - q^2 + 2M\nu$$
$$= q^2(\omega - 1) + M^2, \tag{3}$$

where $\omega = 2M\nu/q^2 = 1 + (W^2 - M^2)/q^2$ is the dimensionless scaling variable, and s the square of the total center-of-mass energy. Another variable often used is the equivalent real photon energy (K) needed to photoproduce a final hadronic system W; it is also thought of as the inelasticity of the collision $(K = 0$ for an elastic collision), where

$$K = \nu - q^2/2M$$
$$= (W^2 - M^2)/2M. \tag{4}$$

Thus we see that there are two independent variables ν and q^2 which can be obtained from the two experimental parameters E' and θ, the final energy and scattering angle of the muon.

Dynamically, only the lepton side of the Feynman graph is known; recent models have been guidelines in trying to understand the hadron vertex. The double differential cross section obtained using quantum electrodynamics for the first-order diagram is [10,11]

$$\frac{d^2\sigma}{dq^2 d\nu} = \frac{2\pi\alpha^2}{|\vec{p}|^2 q^4}\{(q^2 - 2m^2)W_1(q^2\nu)$$
$$+ [2E(E - \nu) - \tfrac{1}{2}q^2]W_2(q^2, \nu)\}, \tag{5}$$

where α is the fine-structure constant, m is the mass of lepton, and W_1, W_2 are the unknown structure functions which depend upon the properties of the target nucleon and can be represented as a function of two variables, q^2 and ν. If one neglects the lepton mass, which can be done in high-energy collisions, Eq. (5) becomes

$$\frac{d^2\sigma}{dq^2 d\nu} = \frac{4\pi\alpha^2}{q^4}(E/E')[2\sin^2(\tfrac{1}{2}\theta)W_1(q^2, \nu)$$
$$+ \cos^2(\tfrac{1}{2}\theta)W_2(q^2, \nu)]; \tag{6}$$

for the small-angle range of the present study, W_2 is observed. Another way of describing the inelastic lepton scattering as an analog of photoproduction is given in terms of Hand's notation [12] σ_T and σ_S, where σ_T and σ_S represent the total

absorption of transverse and longitudinal photons, respectively, and are given as

$$\sigma_T + \sigma_S = \frac{4\pi^2\alpha}{K}(1 + \nu^2/q^2)W_2$$

and (7)

$$\sigma_T = \frac{4\pi^2\alpha}{K}W_1 .$$

Observing W_2 is equivalent to observing $\sigma_T + \sigma_S$. Using Eq. (7) with Eq. (5), one can arrive at the following:

$$\frac{d^2\sigma}{dq^2 d\nu} = \Gamma(q^2, \nu)(\sigma_T + \epsilon\sigma_S) ,$$

where

$$\epsilon = 1 / \left[1 + \frac{q^2 - 2m^2}{2E(E-\nu) - \frac{1}{2}q^2} \left(\frac{q^2}{q^2 + \nu^2} \right) \right]$$ (8)

and

$$\Gamma(q^2, \nu) = \frac{\alpha K}{|\vec{p}|^2} \frac{1}{2\pi q^4} \left[(q^2 - 2m^2) + \frac{2E(E-\nu) - \frac{1}{2}q^2}{1 + \nu^2/q^2} \right] .$$

Both of these forms W_2 and $\sigma_T + \sigma_S$ are the same as observing, in Perl's[13] notation, the expression $\sigma_{exp} = \sigma_T + \epsilon\sigma_S$, since for the small angles found in this work $\epsilon = 1$. In the limit of $q^2 \rightarrow 0$, the transverse cross section approaches the total photoabsorption cross section $\sigma_{\gamma p}$ [i.e., $\sigma_{exp} \rightarrow \sigma_T \rightarrow \sigma_{\gamma p}(\nu)$ since $\sigma_S \rightarrow 0$]. Explicitly, the forms for σ_{exp} and W_2 are hinted at by the parton and vector-dominance models, giving rise to some guidelines for analysis. From the vector-dominance model,[4]

$$\sigma_{exp} = \sigma_{\gamma p}(K)F_N(q^2),$$

where (9)

$$F_N(q^2) = (1 + q^2/m^2)^{-N}, \quad N = 1 \text{ or } 2$$

and $N = 4$ is the form for elastic scattering, while the parton model predicts

$$\nu W_2 = F(x) ,$$

where (10)

$$x = q^2/2M\nu$$

and these forms are tested in the text.

Within the last couple of years hadron-induced one-body[14] as well as N-body[15] inclusive reactions have been studied intensively as a source of information on the mechanism of multiparticle production at higher energies. For real-photon-induced one-body inclusive (pion) reactions, very few data are available,[16,17] while practically no data are available for electron- or muon-induced reactions, i.e., $\mu + \text{nucleon} \rightarrow \pi + \text{anything}$. The transverse (p_t) and longitudinal (p_l) momentum spectra for muon production data are compared

with hadron- and photon-induced inclusive reactions with the theoretical prediction from the fragmentation and parton models in mind. The essential feature of these models is called factorization, where the p_t and p_l spectra are supposed to become independent, and this prediction, as well as a detailed analysis of p_t and p_l distributions, are discussed in the text.

III. EXPERIMENTAL OBSERVATION AND DATA ANALYSIS

Two stacks consisting of 75 pellicles of Ilford G-5 emulsion (dimensions $10 \times 15 \times 0.06$ cm^3) were exposed to 10.1- and 15.8-GeV/c positive and negative primary muons, respectively, at BNL. The momentum spread of the primary beams is shown[18,19] in Fig. 2. The beams were parallel within 1 mrad to the plane of the emulsion surface with an estimated divergence of 8 mrad, and their purities were one pion in 10^6 or 10^7 muons, with both fluxes being 5×10^5 muons/cm^2. Each pellicle was area-scanned and events with at least one evaporation track were found by this technique and recorded if the following were observed:
(i) a light straight track (muon track) approximately parallel to other primary tracks led into the interaction; (ii) all the secondary tracks and the light primary tracks came from the same vertex. About 7000 events were recorded[20] from both the stacks. The selected events were classified according to the well-known nomenclature for black, grey, or light tracks:
(a) For light tracks, $g_s \leqslant 1.5g_0$, where g_s is the number of grains per 100 μ of secondary track and g_0 is the number of grains per 100 μ of the primary track;
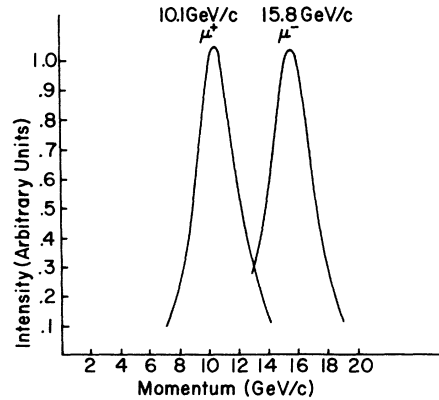(b) for grey tracks, $1.5g_0 < g_s < 2.5g_0$;

FIG. 2. Muon momentum spectrum of the filtered beams as measured by the Columbia-Rochester-BNL group.

(c) for black tracks, $g_s > 2.5g_0$.

The visual selection criteria used to qualify individual events is only a preliminary procedure, and many rigorous tests were applied to reject the background events produced either by cosmic rays or by the secondary tracks produced in other interactions. The selection criteria were the following: (i) The primary muon track should not make an angle greater than 8 mrad with the direction of the incident beam; (ii) the primary track, when traced back to ~1 mm, should be flat and straight and have the same dip angle as the incident beam; (iii) the grain density g_0 of the primary track was measured on a 5-mm length of track to make sure that it corresponded to other primary tracks measured at the same depth. Under these stringent selection criteria, about 1300 events were selected for muon-nucleon inelastic interactions from both the beams. The angle of the outgoing muon was determined from the coordinates of the primary and the secondary muon tracks. The space angles were measured very accurately, i.e., $\theta \sim 0.5$ mrad, by a Koristka scattering microscope, to which was attached a filar micrometer that could be read to an accuracy of 0.2 μ. The secondary particles were identified from measurements of $\tilde{p}\beta c$ and blob counts. The grain densities (g) were obtained from the well-known expression blobs = $ge^{-\alpha \ell}$, and were normalized to the grain density of the primary muon at the same average depth as the secondary particle. With this procedure any error due to nonuniformity of blob density from place to place in the emulsion stack was eliminated. Thus, the identity of the secondary particles was determined by the well-known[21] g^*-$\tilde{p}\beta c$ method by using the Sternheimer energy-loss relation and the measurements of relative grain density and momentum, or by the range-energy relation wherever it was possible. Essentially, the ionization and multiple Coulomb scattering were measured and were used to obtain the masses for all grey and light secondary tracks in each of the events as long as there was a sufficient length of track. For the dimensions of the pellicles used, the required track length was obtained for dip angles less than 30°. Whenever it was considered desirable, the secondary tracks were followed from pellicle to pellicle until they stopped in the emulsion. The track-following technique gave us an independent way of identifying the secondary particles (π, K, p, and Y) uniquely, and thus their energy values were determined from their ranges.

Theoretical curves for g^* vs $\tilde{p}\beta c$ were drawn for each particle (μ, π, K, p, etc.) produced in the muon interaction for 10.1- and 15.8-GeV/c incoming momentum. When using these curves,

there were certain ranges of g^* and $\tilde{p}\beta c$ where identification was ambiguous. For some points the errors involved were large and a choice was made in favor of the most probable particle. From photoproduction data, it is known that a pion or proton is more probable than any of the strange particles, and this criterion was adopted in identifying tracks.

A possible source of contamination in our data is the quasielastic scattering of muons in the heavy nuclei of the emulsion. In order for quasielastic scattering to contribute to our data, the primary muon must transfer enough energy to cause the evaporation of at least one nucleon, and the minimum energy transfer to cause this is about 20 MeV. This energy transfer corresponds to muons with a quasielastic scattering of about 17 mrad. Events with two or more prongs involve an energy transfer of 120 MeV or more, which corresponds to a quasielastic scattering of over 50 mrad. This angle is larger than most of the space angles measured in this experiment, and we can therefore confine possible contamination from quasielastic scattering to the one-prong event. From the kinematics of elastic and quasielastic scattering, we have $q^2 = 2M$ and $q^2 = 2M^*$, respectively, where M is the mass of target nucleon and M^* ($M^* = M/1.3$) is the effective mass of a bound nucleon. Any of our events which satisfy this relation were omitted from the present analysis.

From the above selection criteria we eliminated the elastic as well as quasielastic events. However, in the above discussion the selection of events was made under the assumption that a high-energy muon interacts with only one nucleon, and the possibility of an inelastic collision with the entire nucleus was not considered. This type of collision would be a giant resonance[19] production where the entire nucleus participates in the interaction and returns to the ground state by ejecting one nucleon, which generally comes off approximately at right angles to the primary beam direction. This type of inelastic collision is characterized by an energy transfer of about 15 MeV, giving one black track, and it will show no appreciable scattering of the muon. Thus, some of the single-prong events are expected to be of this kind. A study of the single-prong events was carried out, and it indicated that about 75% of the (1 + 1) type events are from giant resonances. These events were also eliminated from the discussion in the rest of this paper. Coincident background events from cosmic-ray stars were easily separated from the muon angular measurements, since a cosmic-ray star will show no deflection of the continuation muon.

Before we discuss our results, we may mention that the scanning efficiency was about 70% for multiple prongs and 35% for single-black-prong events. It may be stated, however, that the low efficiency from single-prong events has no great effect on the cross-section values used in the next section, as most of these (75%) are from the giant resonance and are rejected as not being inelastic collisions with single nucleons.

IV. RESULTS

Figure 3 gives the kinematic space of q^2 vs ν for 10.1- and 15.8-GeV/c positive and negative muons. The solid line represents scattering by a free nucleon, while the dashed line represents the kinematics for a bound particle with an effective mass of 1/1.3 of a proton rest mass. Only one event falls above the elastic limit. In those cases where we could not determine the energy of the outgoing
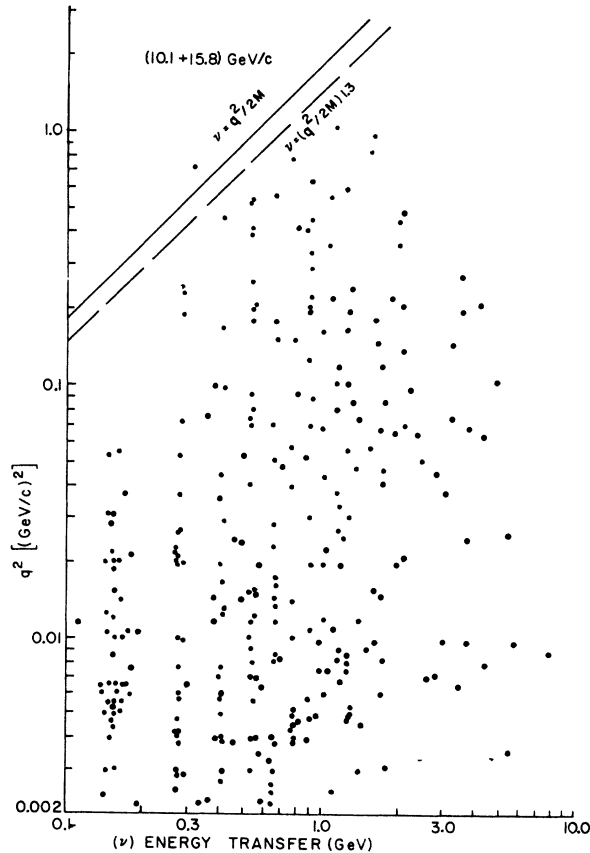
muons directly, we obtained a lower limit on ν by using the multiplicity of each event in conjunction with the nuclear evaporation model. This limit arises since only visible shower tracks were used
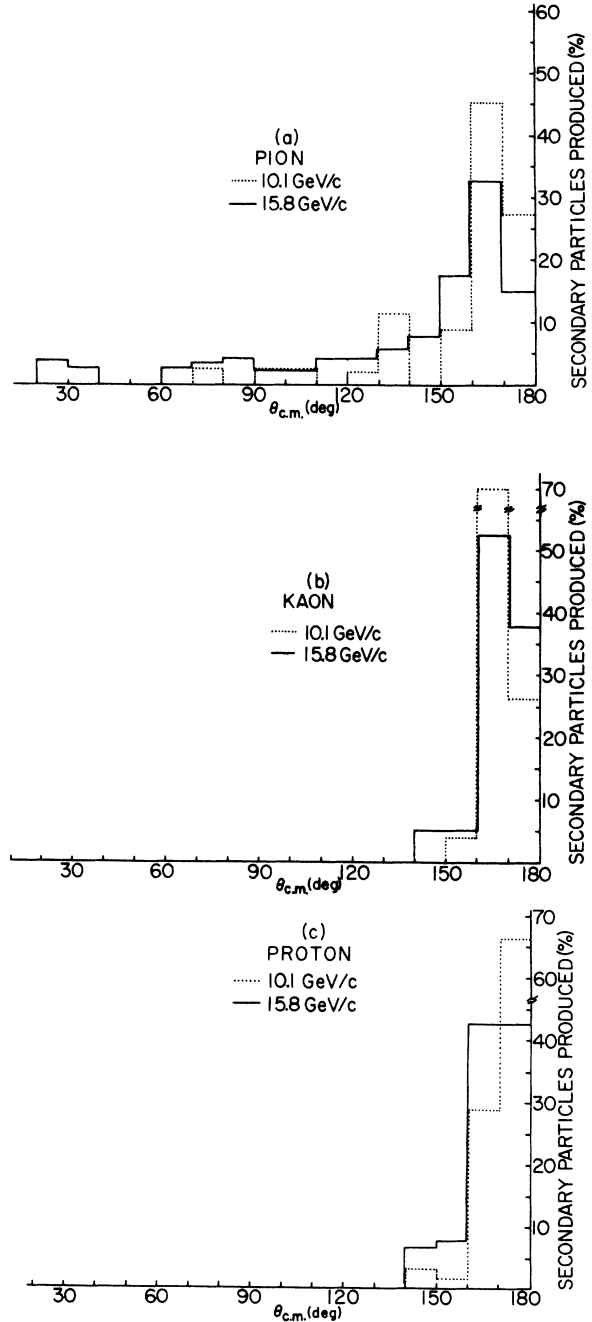
FIG. 3. Plot of the square of the transferred four-momentum q^2 versus transferred energy ν for 10.1- and 15.8-GeV/c muon beams together. The solid line ($\nu = q^2/2M$) is for elastic interaction with a free proton. The dashed line [$\nu = (q^2/2M)1.3$] corresponds roughly to scattering by a proton bound in a nucleus.

FIG. 4. Angular distribution of secondary particles produced by 10.1-GeV/c positive muons (dotted line) and 15.8-GeV/c negative muons (solid line), (a) for pions, (b) for kaons, and (c) for high-energy ($E_p > 25$ MeV) protons.

and no attempt was made to account for neutral shower particles. This method assures one that the sample is free from quasielastic events. For the 10.1-GeV/c beam the energy of practically all of the outgoing muons was determined by direct scattering measurements, while for the 15.8-GeV/c beam the energy ν was determined partly by scattering and partly by the evaporation model.[22] This technique was checked for the low-energy beam (10.1 GeV/c) and was found to be quite satisfactory.

A. Secondary Particle Production

After knowing the energy and angle of the out-going muons, one is interested in the study of secondary particles, i.e., in their identities, the production angle with respect to the primary particles, the energy spectrum, and their method of production. We may mention that although there have been a number of papers dealing with deep-inelastic interactions in high-energy lepton-nucleon interactions, none of these experiments has studied the secondary particles. This is because their experimental arrangement was such that they detected only the secondary lepton at a predetermined laboratory angle. In comparison, our experimental technique allows observation of the entire event, and preliminary results of the first work in secondary particle production were presented earlier from our laboratory.[20] Single-pion photoproduction has been shown to occur principally through the first nucleon resonance, and the angular distribution is predominantly in the backward direction in the c.m. system at all energies corresponding to this resonance.[23] There is also a backward enhancement in the angular distribution in the c.m. system of pions produced by virtual photons which are associated with the present incoming muon beams, i.e., 10.1- and 15.8-GeV/c. The angular distribution of pions was compared with pion-photoproduction experiments and theory,[20] and the general form was found to agree reasonably well. The distributions of pions, kaons, and high-energy protons ($E_p > 25$ MeV) are shown in Figs. 4(a), 4(b), and 4(c), respectively. The protons and kaons are strongly peaked in the backward direction with a complete absence of any forward particles. The pions are also peaked backward with about 15–20% in the forward direction, indicating that the pions come off at higher velocities in the laboratory system. There is more spread of the angular distribution of pions towards the lower angles with the 15.8-GeV/c muon beam than with the 10.1-GeV/c muon beam. The pion production is thought to come from the (3, 3) resonance, and this mechan-

ism would predict a strong backward peak in the c.m. system. However, there are some pions in the forward direction, and one can say that a number of pions are also produced directly through
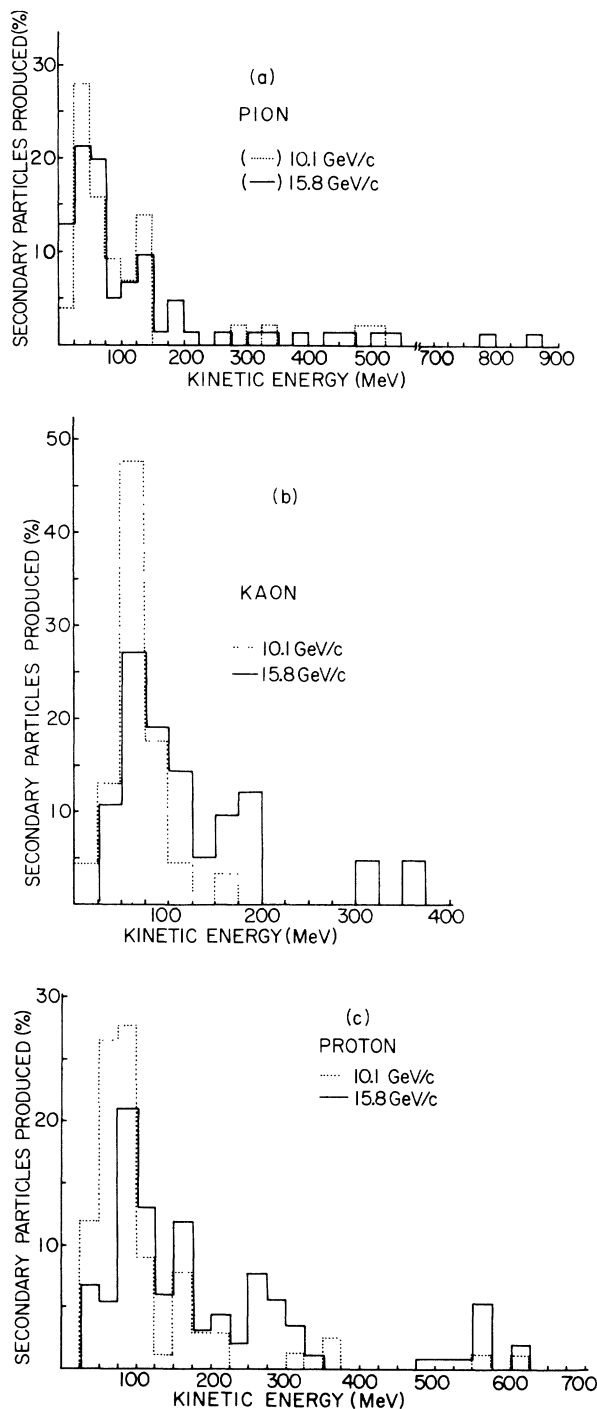

FIG. 5. Energy distribution of secondary particles produced by 10.1-GeV/c positive muons (dotted line) and 15.8-GeV/c negative muons (solid line), (a) for pions, (b) for kaons, and (c) for protons.

TABLE I. Cross-section values for muons on nucleons. All values include geometrical correction and scanning biases.

Process	3.0 GeV/c	5.0 GeV/c	σ (μb/nucleon) 8.0 GeV/c	10.1 GeV/c	15.8 GeV/c
Total inelastic muon–nucleon	4.05 ± 1.4	4.9 ± 0.8	5.98 ± 2.1	7.75 ± 1.6	9.63 ± 1.7
Charged-pion production	$\cdots$	0.85 ± 0.2	$\cdots$	1.07 ± 0.58	1.09 ± 0.21
Charged–strange-particle production	$\cdots$	0.25 ± 0.15	$\cdots$	0.90 ± 0.30	0.49 ± 0.08

multiple-pion-production events rather than through resonances. An analysis of these data for the production of the "Roper" meson (1470 MeV) which should be prominent at extremely low-momentum transfer was presented elsewhere[20] along with the discussion of the other nuclear resonances (1238 and 1512 MeV). Some of the strongly interacting shower particles which are produced are reabsorbed and never get out of the emulsion nuclei. The production goes down rapidly as the mass number increases. This was supported by the experiment of Boyarski et al.,[24] who measured the cross section for the photo-production of single pions and kaons from complex nuclei using 8- and 16-GeV photons. Their range of four-momentum transfer was the same as in our experiment, so we can expect large absorption from the heavy nuclei, which compose about 25% of the emulsion by number.

The kinetic energy of the secondary particles was found from their measured value of $p\beta c$ and is given by $T = \frac{1}{2}\{ p\beta c + [(p\beta c)^2 + (2mc^2)]^{1/2}\}$. The energy spectra of pions, kaons, and protons for 10.1- and 15.8-GeV/c muons is shown in Figs. 5(a), 5(b), and 5(c), respectively. The pion, kaon, and proton energy spectra extend up to 160 and 500 MeV, 100 and 400 MeV, and 225 and 675 MeV, with their peak values at 30 and 50 MeV, 70 and 75 MeV, and 85 and 100 MeV in the 10.1- and 15.8-GeV/c muon beams, respectively.

To calculate the total inelastic cross section, we took into account the scanning bias and the scanning efficiency, and the results are shown in Table I.[25,26] Also shown in Table I are the partial cross sections for the production of the secondary particles, and here we have to make a geometric correction (resulting from a dip-angle cutoff) besides the scanning corrections. The correction factor for the number of tracks of different particles produced, but not used due to the stringent selection criteria of dip angles of secondary tracks, is given by $\frac{1}{2}\pi/\sin^{-1}(\sin d_{max}/\sin\theta_L)$ for $\theta_L \geq d_{max}$, where d_{max} is the maximum dip angle (30°). θ_L is the space angle of the secondary particles measured relative to the primary muon. For the calculation of the particle cross sections,

we did not take into consideration any nuclear effects, although the data in Table I indicate a large absorption of secondary particles. The cross-section data indicate that there are a large number of events with no visible secondary produced particles. The cross section for ρ^0 production was very small ($\sim 7 \times 10^{-32}$ cm^2/nucleon).

Another important parameter to measure for secondary particles is the transverse momentum, which is Lorentz-invariant. Shown in Fig. 6 is the transverse momentum distribution of the produced pions with a long tail going up to 500 MeV/c. The curve has been corrected geometrically for steepness of track and momentum distribution and there should be no bias in the observed spectral shape. This curve was fitted to both a Hagedorn[27] distribution (i.e., $N \approx H_1 p_t^{3/2} e^{-p_t H_2}$) and to a Boltzmann ($N \approx B_1 p_t e^{-p_t^2 B_2}$), where $H_1 = 173$, $H_2 = 1.82$, $B_1 = 52.7$, and $B_2 = 0.548$; one sees that the Hagedorn distribution gives the better fit, giving a most probable value of 100 MeV/c. The average transverse momenta for pions, kaons, and protons are 178 ± 35, 225 ± 45, and 361 ± 12
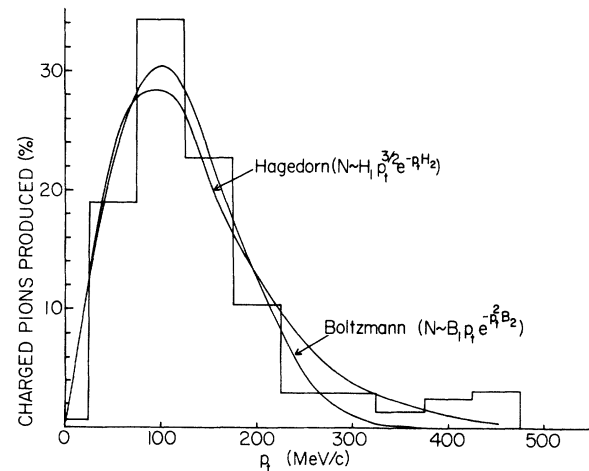

FIG. 6. Distribution of transverse momentum p_t of all charged pions produced by 10.1- and 15.8-GeV/c muons interacting with nucleons. This distribution is compared to the curves given by the Hagedorn ($N \sim H_1 p_t^{3/2} e^{-p_t H_2}$) and Boltzmann ($N \sim B_1 p_t e^{-p_t^2 B_2}$), distributions, where $H_1 = 173$, $H_2 = 1.82$, $B_1 = 52.7$, and $B_2 = 0.548$.

MeV/c, respectively. These values are found to be in agreement with other observations made in emulsions where the projectiles were protons.[28]

B. Inclusive Reaction Study

It has been shown that Yang's hypothesis of limiting fragmentation is approximately true in several reactions involving hadrons. Recently, from the study of the dependence of the high-energy photoabsorption cross sections on the size of the target nucleus, it became clear that the photons do not behave in a purely electromagnetic manner[29] but rather are absorbed more like a strongly interacting particle in passing through a nucleus. We know also that γp reactions have many features in common with πp interactions; i.e., the average transverse momentum is small, the total cross sections have very similar energy behavior, and many of the same resonances are observed in both cases. These observations are approximately explained by the notion of vector dominance, as the photon has the same quantum numbers as the vector mesons. On account of the hadronlike properties of the photon, one may think that the limiting fragmentation may also be a property that γp has in common with πp, pp, Kp, and perhaps other hadron-hadron collisions.

Subsequently, photoproduction of π^- mesons has been reported by two groups working at SLAC. Swanson et al.,[16] used a bremsstrahlung beam and a streamer chamber and could not determine the incident photon energy precisely. An experimental difficulty arises from the fact that the photon beam contains all energies up to 18 GeV, and therefore the energy of a given event is not exactly determinable if neutral particles are emitted. Instead, they separate the data into groups with different ranges of "visible" energy (5.5–15 GeV), the sum of which is the energy of the charged particles in the laboratory. The second photoproduction experiment by Moffeit et al.,[17] employed a laser beam impinging on a high-energy electron beam. Back-scattered photons from these collisions then traversed a bubble chamber. In this way, monochromatic photons of 2.8, 4.7, and 9.3 GeV were obtained. A comparison between the preliminary photon data and the hadron data shows that a photon behaves like a hadron in two-body processes. If the photon indeed behaves like a hadron, it can be used as an extra hadron to check various predictions like scaling or projectile independence. The use of a polarized photon beam gives us the first opportunity to learn something about the spin correlations[30] in inclusive reactions.
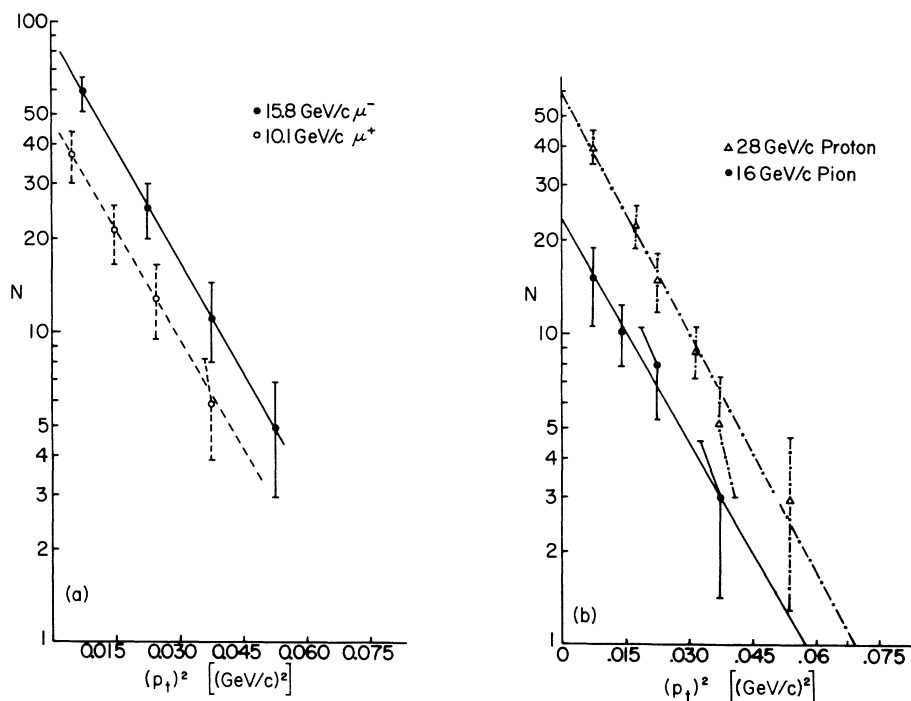

FIG. 7. $p_t{}^2$ distribution for all the charged secondary pions produced in (a) muon-nucleon interactions at 10.1 GeV/c (---) and at 15.8 GeV/c (—); (b) in pp interactions at 28 GeV/c (-··-) and in πp interactions at 16 GeV/c (—), both in the same range of $p_t{}^2$ distribution.
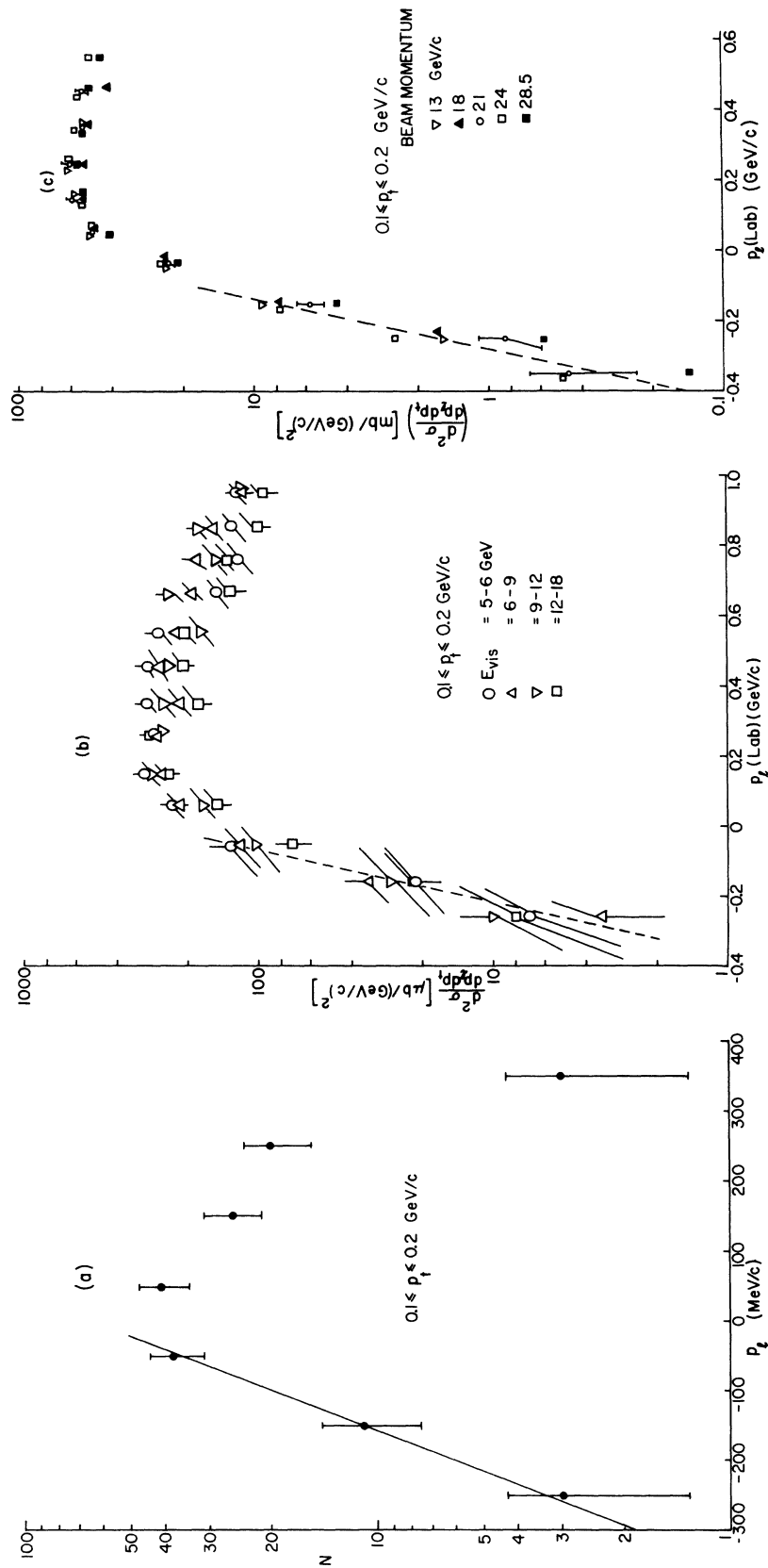
FIG. 8. p_l distribution for all charged secondary pions in the laboratory system for the range $0.1 \leq p_t \leq 0.2$ GeV/c, (a) from muon beams together, (b) from γp interactions at 5–18 GeV, and (c) from pp interactions at 13–28.5 GeV/c.

Inelastic scattering of a lepton on a nucleon is an unexplored interaction, especially for the study of muon-induced inclusive reactions, i.e., μ +nucleon → π +anything. We know of no published data for secondary particle production (e.g., pion, kaon, etc.) with high-energy muon-nucleon interactions except from our own laboratory.[20] So it is highly desirable at this stage to study the inclusive reactions for high-energy (10.1- and 15.8-GeV/c) muon interactions on nucleons for secondary pion production and to compare them with photoproduction γp (5–18 GeV) experiments as well as with the hadronic experiments[16] with pp (28 GeV/c) and[31] πp (16 GeV/c). Preliminary results were presented earlier.[32] An important feature of the inclusive reaction is the distribution of the transverse momenta, which seems to be limited to a few hundred MeV/c nearly independent of the energy. We divided all our events from each beam into two groups, i.e., with $|p_t|$ < 0.075 MeV/c and with $|p_t|$ > 0.075 MeV/c, and found that the two p_t^2 curves have the same shape and slope. Shown in Fig. 7(a) is the p_t^2 distribution for pions produced in muon-nucleon interactions at 10.1 and 15.8 GeV/c for all p_l and W values. This is compared with pions produced in proton-nucleon interactions at 28 GeV/c and pion-nucleon interactions at 16 GeV/c, as shown in Fig. 7(b), with the same range of p_t^2 values as in the muon-nucleon interactions. The slope of the curves in Fig. 7(a) is about 58 ± 7, and this compares to a slope of 60 found over the same range where protons were used as projectiles. Thus agreement in the shapes of the distributions within the chosen energy interval is remarkably good, indicating the independence of the value of the incoming momentum as well as the type of incoming particle. There is no detailed information available for pion-production events from γp interactions for the small range of p_t^2 values [i.e., 0 to 0.075 (GeV/c)^2] of our experiment, and hence we cannot compare the shape and slope of the curve in Fig. 7(a) with either of the two photon experiments mentioned earlier.[6,33]

Another parameter that we can compare is the laboratory longitudinal momentum (p_l). In the c.m. system p_l^* is given in terms of Feynman's variable $x = 2p_l^*/s^{1/2}$. According to Yang's hypothesis of limiting fragmentation, the target fragments with negative x (in the c.m. system of virtual photon and target nucleon) should have the same distribution as for a real-photon; pion- or proton-induced process. Since pion-production data in other interactions are available in the laboratory system, and the region of backward pions is presumably richer in proton fragmentation than the entire p_l range, we show in Fig. 8(a)
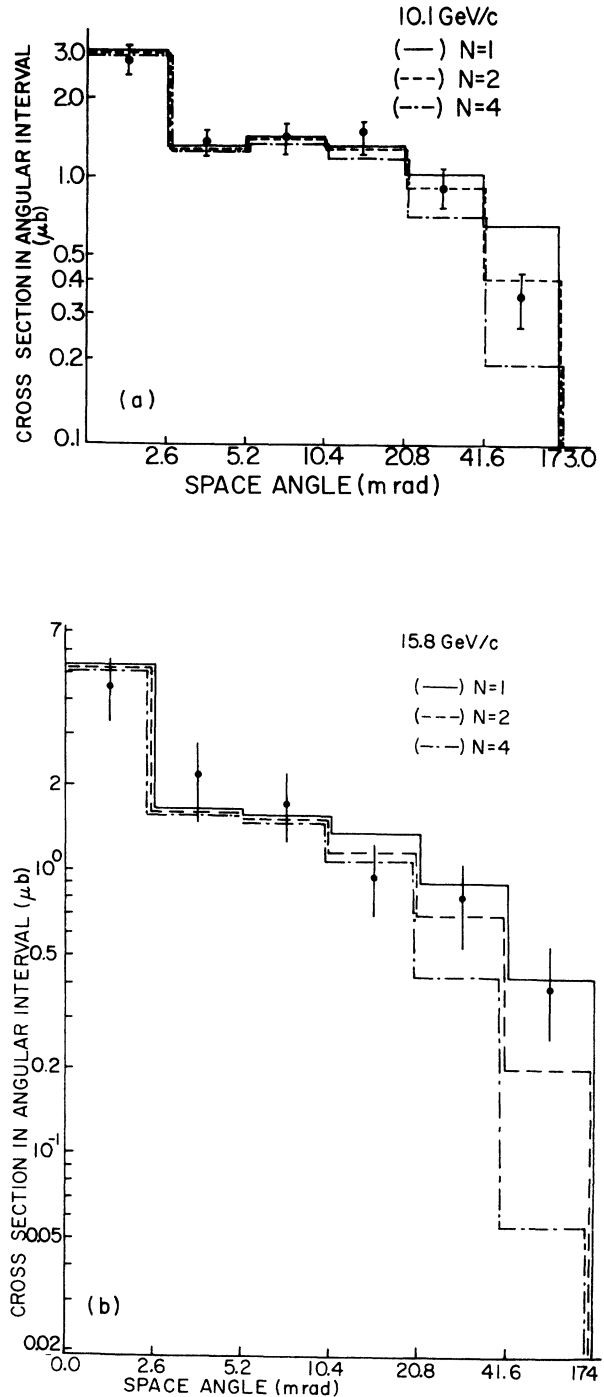

FIG. 9. Total cross section within an angular interval $\Delta\theta$, (a) for 10.1-GeV/c muons and (b) for 15.8-GeV/c muons. The theoretical curves were obtained by integrating $d^2\sigma/d\Omega E'$ over the range of E' and the interval in question. The three different forms are for $N =1$, 2, and 4 used for σ_{exp} in the theoretical calculations. The last bin in the histogram includes the rest of the events.

the distribution of p_l in the laboratory system for pions produced in 10.1- and 15.8-GeV/c muon-nucleon interactions. This is compared with pions produced in γp interactions at 5–18 GeV shown in Fig. 8(b) and pp interactions at 5–18 GeV shown in Fig. 8(c), respectively, within the same range of p_t (i.e., $0.1 \leqslant p_t \leqslant 0.20$ GeV/c). The data in Figs. 8(b) and 8(c) for $p_l < 0$ (target region) extend approximately up to the same value of p_l (i.e., ~ -0.3 GeV/c) as shown in Fig. 8(a) for the same p_t range interval, i.e., $0.1 < p_t < 0.2$ GeV/c. Here one sees that the slopes of the curves in Figs. 8(a), 8(b), and 8(c) are 11.9 ± 2.4, 12, and 13.1, respectively. The negative values of p_l range from 0.0 to -0.30 GeV/c. We conclude that the shape and the slope of the curves for p_t^2 and p_l distributions for inclusive pion-production reactions in muon-nucleon interactions at 10.1 and 15.8-GeV/c are the same as those for hadronic reactions, indicating that the muon in muon-nucleon interactions, at least for the negative values of p_l, behaves like a hadron.

C. Test of the Vector-Dominance Model (VDM)

1. Partial Cross Section as a Function of Angle

To test the vector-dominance predictions two plots were made, one involving partial cross sections in an angular interval and the other involving integral cross sections against q^2. The partial cross section as a function of the angle of the continuation muon relative to the primary muon direction provides an accurate means of comparing the experimental data with theory. It was pointed out earlier in this paper that emulsions have very high spatial resolutions and one can in fact measure angles down to half a milliradian. The partial cross section is given by $\Delta \sigma = [n(\Delta\theta)]/NIV$, where $n(\Delta\theta)$ is the number of events in the angular interval $\Delta\theta$ corrected for scanning efficiency, N is the number of target nucleons per cubic centimeter, $N = 1.94 \times 10^{24}$ nucleons/cm^3; V is the volume of the target material; and I is the intensity of the muon beam. Thus Fig. 9(a) displays partial cross sections in an angular interval where the data points were obtained by counting the number of events in an angular range and computing a cross section for that range of θ from the relation given above. The total errors were found by adding an uncertainty error of 10% in the scanning efficiency to the statistical error.

The theoretical curves were obtained first by integrating out the energy of the continuation muon in Hand's[12] form of the inelastic Rosenbluth formula,

$$\frac{d^2\sigma}{d\Omega dE'} = \Gamma_T(E', \theta)\sigma_{\exp}(K, q^2), \qquad (11)$$

where $\Gamma_T(E', \theta)$ represents all the kinematical factors given in Sec. II. The partial cross section for each angular interval was then obtained by integrating the angle over each of these intervals by performing a numerical integration of the differential cross section with the help of the Gaussian quadrature technique.[34] We used the value of $\sigma_{\gamma p}$ as computed by Cone et al.[35] up to 5 GeV, and thereafter we took $\sigma_{\gamma p}$ to be constant ~ 125 for the continuum value. The three theoretical values arise from the use of three forms for $\sigma_{\exp}$ $= \sigma_{\gamma p}(K)(1 + q^2/m_\rho^2)^{-N}$, where $N = 1, 2$ represents the VDM model while $N = 4$ represents the expression for the elastic form factor. Experimental data and the theoretical curves for 10.1- and 15.8-GeV/c muons are shown in Figs. 9(a) and 9(b), respectively. In either of these two diagrams the three theoretical curves are essentially the same, up to an angle of 10 mrad, which is consistent with our data. It is clear from both the figures that the data points do not separate the three forms until the last two bins. It is seen that the muon data fit the $N = 1$ form best, and this is in agreement with the muon experiments of Braunstein et al.,[13] revealing that the small-angle data follow the same form as the large-angle data observed at SLAC.[2] Since they did not observe small angles ($\theta < 30$ mrad), the present experiment complements theirs.

2. Integral Cross Section as a Function of q^2

Once again we make use of Eq. (11) in which the variables Ω and E' are changed to q^2 and ν. The experimental points for this plot were found by adding up the number of events with q^2 greater than some specified value, and the cross section was computed for each case from the expression given earlier. These cross sections were then plotted against their respective values of q^2 and are shown in Figs. 10(a) and 10(b) for 10.1 and 15.8 GeV/c, respectively. The corrections and error analysis applied here to the observed points are the same as mentioned in the previous case. Theoretical curves were calculated for each of the forms previously chosen for $\sigma_{\exp}(K, q^2)$. The curves were obtained by integrating the differential cross section over ν and q^2. The integral was performed by first integrating out the final energy E' of the muon and then integrating from the chosen value for q^2 as the lower limit to the largest value of q^2 found in this study. We have found that the integration was not sensitive to the values of maximum q^2 used in the equation. The data in Fig. 10(a) for a 10.1 GeV/c muon indicate diver-
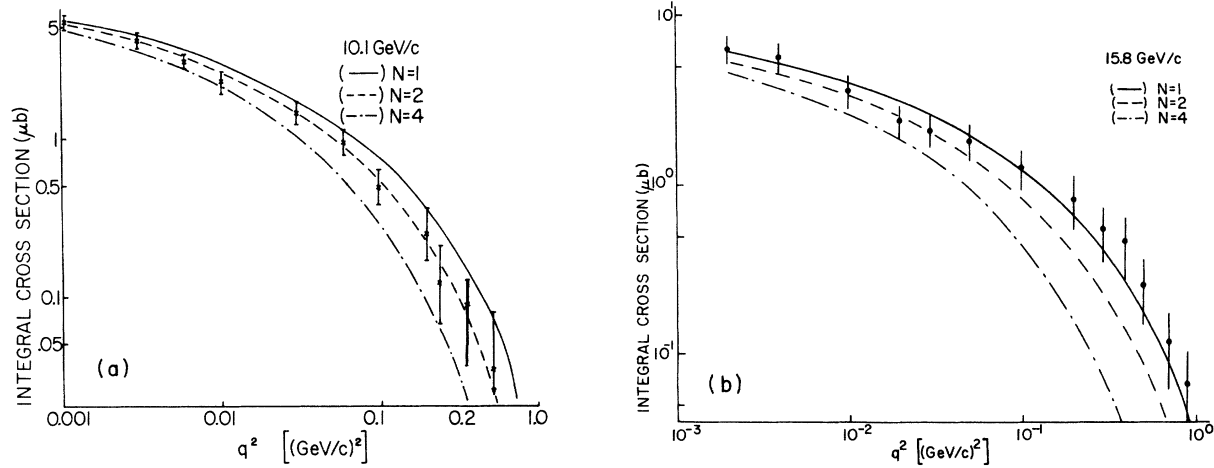
FIG. 10. Integral cross section versus q^2 for (a) 10.1-GeV/c and (b) 15.8-GeV/c muon beams. The theoretical curves were obtained for three different forms used for σ_{exp} in the theoretical calculations corresponding to $N = 1$, 2, and 4.

gence from the inverse fourth power around q^2 $\simeq 0.2$ (GeV/c)^2 and follow the inverse quadratic for the rest of its range. This result is in agreement with the work of Hoffman et al.[36] However, we cannot rule out the inverse linear form due to the error bars. For 15.8-GeV/c muon data one can see in Fig. 9(b) that the data points follow the inverse-linear form, but as the error bars are large, one cannot completely rule out the inverse quadratic form. But one does see from these two plots in Figs. 10(a) and 10(b), as well as from the previous two plots in Figs. 9(a) and 9(b), that the inverse fourth power form is completely ruled out. Our data agree with the electroproduction experiment of Miller et al.[2] as well as with the muon production experiment of Braunstein et al.[13] This agreement is also within the realm of the vector-dominance model. There is no indication of a difference between muons and electrons in the kinematic region explored.

3. Total Cross Section

In Table I we have given the total cross section for different primary energies, and in Fig. 11 is displayed the total observed cross section as a function of energy, where the other data points are taked from the work done in our laboratory. The theoretical curves were obtained by doing the angular and final-energy integrations over their entire range for different values of the primary energy using the three different forms of σ_{exp}. It seems that there is a tendency for the total cross section to follow the inverse fourth power for σ_{exp}. In considering all the data presented, we can say that the total cross section is little affected by events with high q^2 values. Most of the events are

at low q^2, and we have already seen for low-q^2 events that σ_{exp} follows the inverse fourth power, which is similar to the elastic form factor. When we separate the high-q^2 events, which represent a small percentage of the total cross section, our data tend toward a weaker q^2 dependence of σ_{exp}, such as the inverse-linear and inverse-quadratic forms, indicating the importance of the vector-dominance model at such q^2 values.

D. Parton Model

1. Ratio of σ_n/σ_p

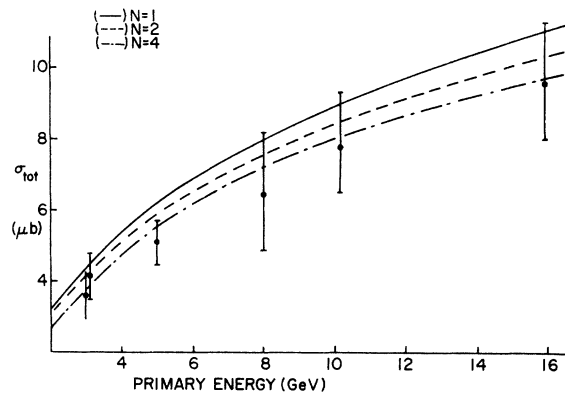There is a more interesting speculation in the prediction of the parton model which indicates[37]

FIG. 11. The total cross section as a function of primary energy. The theoretical curves are for three different forms, i.e., $N = 1$, 2, and 4, for the expression σ_{exp}. The integrations were performed in much the same way as in Figs. 9 and 10 except that the angular integration was done over the whole range.

that $\sigma_n/\sigma_p = 0.8$, where σ_n and σ_p are the cross sections for neutron and proton interactions with the incoming leptons. Since in this experiment there are 1.3 neutrons for every proton, the following expression applies[38]:

$$(\sigma_{tot})_{obs} = (\sigma_p + 1.3\sigma_n)/2.3,$$

and using the theoretical value for σ_p we get $\sigma_n/\sigma_p \simeq 0.8 \pm 0.28$ for all our data, and 0.63 ± 0.31 using the data over the range $\theta \geq 10$ mrad. These values should be taken with caution since our errors are large; however, a more accurate and detailed study of total cross section may reveal interesting results.

2. Particles Produced Along the Direction $\vec{q}$

The parton model[37] and the field-theoretical model[38] both make predictions concerning secondary particles coming out in the direction of $\vec{q}$ (the three-momentum transfer, see Fig. 1). In the parton model[39] the lepton interacts with one of the partons, which bears the initial brunt of the collision, and one expects that particles produced along $\vec{q}$ will possess the parton's quantum numbers. The field-theoretical model[38] is more specific and one should expect that these particles must be protons. The angle made by $\vec{q}$ depends on q^2 and the energy transfer such that

$$(q \cdot p)/|\vec{q}| \, |\vec{p}| = \cos\psi_{\vec{q}}$$

$$= \sin(\tfrac{1}{2}\theta) \simeq 0, \quad \psi_{\vec{q}} = 90°$$

where $\psi_{\vec{q}}$ is the space angle of $\vec{q}$ relative to the primary muon; here we assume that the angle the outgoing muons make with the direction of the primary is practically zero. In the 10.1-GeV/c muon data, out of all the secondary particles observed and measured, ten of them occurred in a 10-degree cone along $\vec{q}$. Seven of them were protons, two were pions, and one was a strange particle. Although the number of observed particles is too small to permit any definite conclusions, the proton space angle does seem to favor the direction of $\vec{q}$ and these results offer some support to the field-theoretical model. The same kind of conclusions were drawn from the 15.8-GeV/c muon data.

E. Test of Scaling at Low q^2

From the general theory of inelastic scattering, we derive the expression for the double differential cross section in terms of the structure functions W_1 and W_2 which is given in Eq. (3) of Sec. II. Bjorken[1] suggested that for large ν and q^2 with ω finite, the function $\nu W_2(q^2, \nu)$ should exhibit the property of scale invariance by a dependence

on only a single dimensionless variable $\omega = 2M\nu/q^2$, instead of on two independent variables q^2 and ν. Furthermore, the universal function νW_2 in the limit of large ω is expected to approach a constant value. The quantity νW_2 for the proton has recently been studied in the so-called deep-inelastic region by MIT-SLAC[2] and DESY[8] collaborations at different angles. When one restricts the region $W \geq 2.0$ GeV, and $q^2 \geq 0.5$ (GeV/c)^2, then the resulting data are consistent with scaling. The curve for νW_2 starts at zero at $\omega = 1$, the position of the elastic peak. When $\omega < 5$, it appears to follow a scaling law $\nu W_2 = F(\omega)$, where $F(\omega)$ is a universal function.

The dynamics underlying the scaling property of νW_2 is not yet clear. We mentioned earlier the various theoretical models which try to explain the scaling; however, none of these is totally satisfying as proposed by Feynman,[5] by Bjorken and Paschos, and by Drell, Levy, and Yan for parton models; and by Sakurai[4] and Fujikawa[33] for vector-dominance models. Bloom and Gilman[6] have suggested that there is a larger range and more rapid approach to scaling behavior if one uses the variable $\omega' = 1 + W^2/q^2 = \omega + M^2/q^2$, where ω' is dimensionless and is the same as ω in the Bjorken limit of ν and $q^2 \to \infty$. νW_2 and W_1 would become independent of q^2, and this is equivalent to the limit $q^2 \to \infty$ if they are studied as a function of q^2 for fixed ω' rather than fixed ω. For a finite value of q^2, there is a difference. In particular, the elastic peak is not at $\omega' = 1$ (recalling $\omega = 1$), but appears at $\omega' = 1 + W^2/q^2 > 1$ and moves to a smaller value of ω' as q^2 increases, just as the other resonances do.[40] From the analysis of their data,
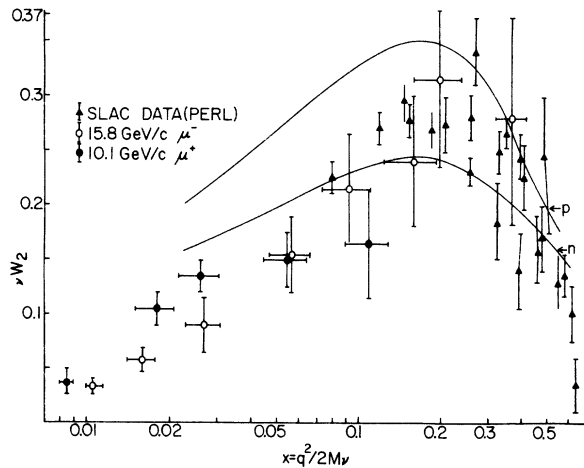

FIG. 12. νW_2 as a function of x ($=1/\omega$). It contains SLAC data (Ref. 13) at low q^2 and the present data at 10.1 and 15.8 GeV/c. The theoretical curves are due to the parton model for protons and neutrons as derived by Gardiner and Majumdar (Ref. 45).

they concluded that resonances are not a separate entity but are an intrinsic part of the scaling behavior of νW_2. On the other hand, by extending local duality and scaling[41] down to $q^2 = 0$ Rittenberg and Rubinstein[42] have shown that the averaging found by Bloom and Gilman is not very good for low values of q^2 either for νW_2 or the differential cross section measured experimentally. They proposed a new scaling variable ω_w which replaces ω', where $\omega_w = (2M\nu + M^2)/(q^2 + a^2)$ and a^2 is a parameter which is adjusted to the data to get an optimum fit with scaling. The scaling variables ω, ω', and ω_w all become equal in the Bjorken limit.

Electron data with low $q^2 \geq 0.5$ and $W \geq 2.0$ GeV are found[8] to be consistent with scaling. For $\sigma_T \gg \sigma_S$ ($R = 0$, see Sec. II), νW_2 appears to level off at ~0.3 when $\omega = 4$. However, the 6° data indicate a downward slope in νW_2 when $\omega \geq 5$ which is not apparent in the 10° data.[2] This indicates that in the functional dependence of νW_2 there exists a weak q^2 dependence, to be taken into consideration specifically at high ω values. The gradual decrease in the function νW_2 for large ω suggests that the photoabsorption cross section for virtual photons falls slowly at constant q^2 as the photon energy ν increases.

Recently Braunstein et al.[13] have obtained muon-nucleon inelastic data at low values of $q^2 \sim 0.3$. Shown in Fig. 12 is the function νW_2 going through a maximum value ~0.26 at $x = 0.2$ (where $x = 1/\omega$

and $0 < x < 1$). The electron-proton inelastic data show that at $x = 0.15$, the values of νW_2 are a little higher, i.e., ~0.33 at the higher q^2 values. However, when we go to large values of $\omega \geq 10$ ($x \leq 0.1$), the data in this region become rather sparse. The value of νW_2 appears to decrease for increasing ω (decreasing x); perhaps the scaling laws are weakly violated at large ω, but this has not been demonstrated convincingly. In the region $\omega > 10$ there are few experimental data and one asks the following: (i) Do the results exhibit scaling behavior, and if so, (ii) are the values of νW_2 in this region equal to the value of νW_2 for $3.5 < \omega < 10$? With the decrease of q^2 the scaling function νW_2 also decreases. We may note that for $q^2 = 0$, νW_2 is also equal to zero, so there must be a region in q^2 where νW_2 does not scale.

In order to test the scaling in the low $q^2 < 0.5$ GeV/c range, which has not been previously tested, it is useful to plot νW_2 for fixed ω' as a function of q^2. For constant ω', scaling behavior should be exhibited in such a plot if νW_2 is independent of q^2 (or W). For this purpose we used the data from 10.1- and 15.8-GeV/c muon beams as shown in Fig. 13. The kinematic region of our data is such that θ is very small. Therefore $\sin^2(\frac{1}{2}\theta) \simeq 0$ and $\cos^2\theta \simeq 1$, and thus from Eq. (6) we have

$$\nu W_2 = (\nu E/E')(q^4/4\pi\alpha^2)d^2\sigma/dq^2 d\nu . \qquad (12)$$
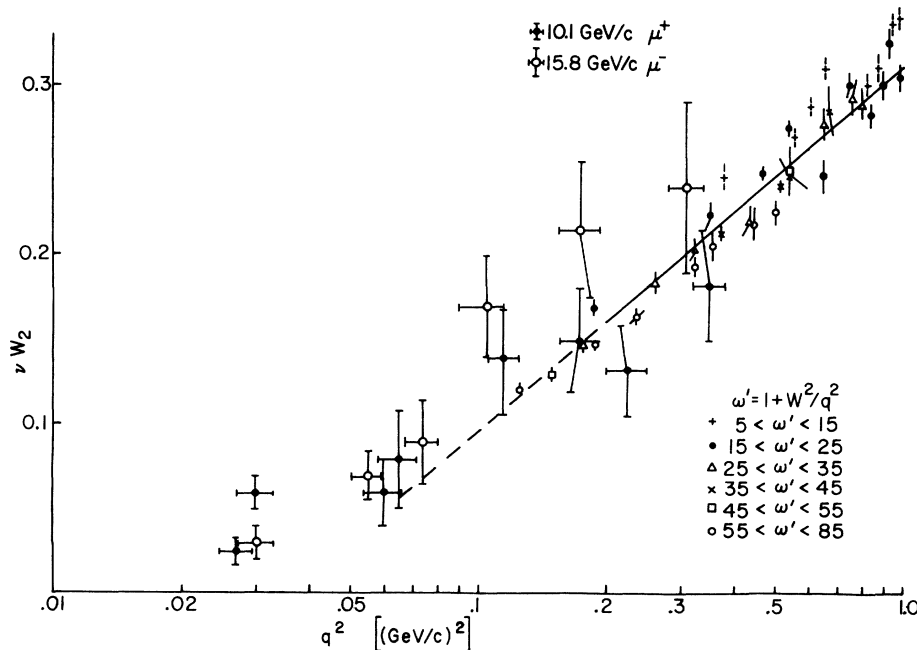
The right-hand side of the above equation was ex-

FIG. 13. νW_2 as a function of q^2. SLAC electron data at 4° are shown along with our 10.1- and 15.8-GeV/c muon data. The theoretical solid curve is due to Sakurai's generalized vector-dominance model for $\omega' > 5$. The dashed lines show the extension of Sakurai's curve.

perimentally measured by choosing a ν and q^2 interval and computing the double differential cross section for those ranges from $\Delta\sigma/\Delta\nu\Delta q^2$ ($\Delta q^2 = q^2$ interval and $\Delta\nu =$ energy transfer ν interval), and using this to compute νW_2 from Eq. (12). In Fig. 13, the value of νW_2 is plotted against the corresponding average value of q^2 for $10 < \omega' < 35$. We have also shown in Fig. 13 the SLAC data[2] at $\theta = 4°$. These results show some dependence on ω' at constant q^2, as well as a strong q^2 dependence. We find that the values of the scaling function νW_2 decrease for values of $q^2 < 0.5$ for the different ranges of the variable ω'. We see that the data extend to very low values of $q^2 < 0.03$ $(\text{GeV}/c)^2$, which have not been reported earlier by any laboratory, and the values of νW_2 decrease from 0.20 to 0.025 (i.e., a 90% decrease) for q^2 values at 0.35 to 0.025, respectively. In the earlier version of VDM by Sakurai,[4] the scaling laws observed by experiments[2] could not be explained. Recently, Sakurai and Schildknecht[43] have proposed a generalized VDM for inelastic electron-proton scattering which takes into account the coupling of the photon to higher-mass vector states. Although the coupling of ρ^0 to the photon is much stronger than that of ω^0 and ϕ^0, one still needs to use the contribution of other vector mesons to explain the experimental results. This model holds for $\omega' > 5$, and Sakurai and Schildknecht did not need "partons" to explain the large cross section and approximate scaling behavior observed in the SLAC-MIT[2] experiment. In Fig. 13 we have shown (solid line) the theoretical curve representing the latest VDM for values of q^2 down to 0.2 $(\text{GeV}/c)^2$.

Figure 14 shows for electrons the values of νW_2 for large q^2 and ν and indicates scaling up to $\omega' \sim 10$. The functional curve $F(\omega')$ starts from

zero at $\omega' = \omega + M^2/q^2 > 1$, rises to a maximum ~ 0.33 at $\omega' = 4$, and appears to remain constant (~ 0.33) for $4 < \omega' \leq 10$. The same figure shows the values of the structure function νW_2 for different values of $\omega' \geq 10$ for 10.1- and 15.8-GeV/c muon beams. The data show the dependence of νW_2 on ω' at small values of $q^2 \leq 0.25$. The values of the structure function (νW_2) at $\omega' = 9$ and 120 are 0.25 ± 0.05 and 0.025 ± 0.008, respectively. The scaling law is perhaps violated at large ω'. Fujikawa[33] has recently proposed a simple phenomenological picture of scaling based on generalized vector-meson dominance by introducing heavy mesons which satisfy the relation $m_V^2 \sim q^2$ which he calls the parton condition. This model is valid only for large scaling parameter ω'. Shown in Fig. 14 are theoretical curves for $\alpha = 1$ and $\frac{1}{2}$, where α is the intercept of the leading Regge trajectory ($\alpha \leq 1$). We see that neither of these two theoretical curves fits our data exactly. Also shown in Fig. 14 are data points of Breidenbach et al.[44] from 6° SLAC data for large ω' values. We see that three points where the values of ν and q were given, although for large energy transfer (5–15 GeV), fit very well with our data.

High-energy muon-nucleon inelastic data are very limited as compared to electron-nucleon inelastic data. Seen in Fig. 12 are the data due to Braunstein et al., at low values of $q^2 \sim 0.3$. Their[13] data give the values of νW_2 for $0.08 < x < 0.6$ ($x = 1/\omega$). We have also plotted our data for both the muon beams and have extended the range of x to 0.0085. We see that the value of νW_2 decreases from 0.30 to 0.03 (i.e., 90%) with the decrease of x from 0.2 to 0.008. This is quite a large change in νW_2 and depends strongly on x. We have also shown (solid line) the theoretical curves obtained for proton and neutron targets by using Gardiner and Majumdar's representation[45] of the parton model. It is quite clear that the data at low x values do not fit with either curve.

Thus we see that in spite of the fact that our data do give glimpses in favor of the parton model or the vector-dominance model, none of these theoretical models mentioned above in Sec. I really works well enough to explain totally the data at low as well as at high values of ω'. Perhaps both sets of data should be treated separately.

Looking at the data in Figs. 10 and 12, we find that the theoretical curves calculated from the parton model[17] and from the VDM (Reference for $\alpha = \frac{1}{2}$) are not in agreement with the present experimental data. Interestingly the effect of both [i.e., pointlike (parton model) and hadronlike (VDM)] interactions of the physical photon seems to contribute even at relatively low q^2 values.
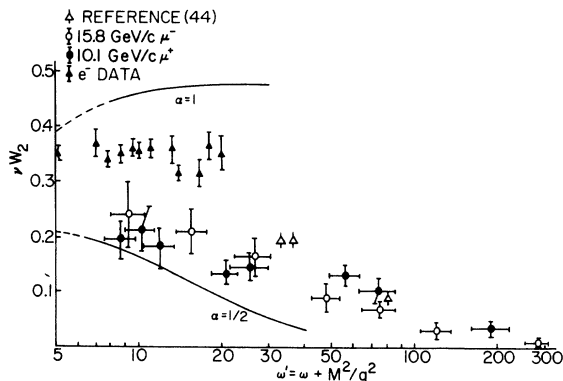

FIG. 14. νW_2 as a function of ω'. SLAC electron data (Ref. 2) are shown along with our muon data at 10.1 and 15.8 GeV/c. The theoretical solid curves for $\alpha = 1$ and $\frac{1}{2}$ are due to Fujikawa's vector-dominance model. α is the intercept of the leading Regge trajectory and is ≤ 1.

Brodsky et al.[46] have used the expression

$$\sigma(\gamma p) = 0.22\sigma \text{ (pointlike)} + 0.78\sigma \text{ (VDM)}, \quad (13)$$

and this two-component picture of photon interactions is applicable to any target. In particular the target could be a nucleus, and by using the "A" dependence expected for VDM[47] (i.e., $\sigma_{(\gamma A)}/\sigma_{(\gamma N)} \sim A^{0.89}$) one finds

$$\sigma_{(\gamma A)}/A\sigma_{(\gamma N)} \sim 0.22 + 0.78 A^{(0.89-1)},$$

which agrees remarkably well with the data[29] for C, Cu, and Pb. Furthermore, it has been found recently[48] that the A dependence of π^0 photoproduction is almost independent of energy (4–10 GeV), in contradiction with vector-dominance predictions.

Thus we see that the scaling observed at SLAC represents the effect of a theory which is not applicable at smaller q^2 and that there is no smooth interpolation between the Regge region and the scaling region. Perhaps a new theory could be developed in which the physics is not discontinuous.

ACKNOWLEDGMENTS

*Present address: Cornell Aeronautical Laboratory, Inc., Buffalo, New York,

[1]J. D. Bjorken, Phys. Rev. 179, 1547 (1969); in Proceedings of the International School of Physics "Enrico Fermi," Course IXL, edited by J. Steinberger (Academic, New York, 1968), p.55.

[2]E. D. Bloom et al., MIT-SLAC Report No. SLAC-PUB-796, 1970 (unpublished), presented at the Fifteenth International Conference on High Energy Physics, Kiev, U.S.S.R., 1970; SLAC Reports Nos. SLAC-PUB-907 and -815 (1970); G. Miller, E. D. Bloom, G. Buschhorn, D. H. Coward, H. DeStaebler, J. Drees, C. L. Jordan, L. W. Mo, R. E. Taylor, J. I. Friedman, G. C. Hartmann, H. W. Kendall, and R. Verdier, Phys. Rev. D 5, 528 (1972).

[3]H. R. Pagels, Phys. Lett. 34B, 299 (1971); T. Akiba, M. Sakuraoka, and T. Ebata, Nuovo Cimento Lett. 4, 1281 (1970); H. Harari, Phys. Rev. Lett. 24, 286 (1970); J. J. Sakurai, ibid. 29, 981 (1968).

[4]J. J. Sakurai, Phys. Rev. Lett. 22, 981 (1969).

[5]R. P. Feynman, Phys. Rev. Lett. 23, 1415 (1969); J. D. Bjorken and E. A. Paschos, Phys. Rev. 185, 1975 (1969); S. Drell and T.-M. Yan, Phys. Rev. Lett. 24, 181 (1970); E. Bloom and F. Gilman, ibid. 25, 1140 (1970); A. suri and D. R. Yennie, Ann. Phys. (N.Y.) 72, 243 (1972).

[6]E. D. Bloom and F. I. Gilman, Phys. Rev. Lett. 25, 1140 (1969); Phys. Rev. D 4, 2901 (1971).

[7]A. suri and D. R. Yennie, Ann. Phys. (N.Y.) 72, 243 (1972).

[8]J. Moritz, K. H. Schmidt, D. Wegener, J. Bleckwenn, and E. Engels, Nucl. Phys. B41, 336 (1972).

[9]J. Benecke, T. T. Chou, C. N. Yang, and E. Yen, Phys. Rev. 188, 2159 (1969).

[10]S. D. Drell and J. D. Walecka, Ann. Phys. (N.Y.) 28, 18 (1964).

[11]R. D. Malucci, SUNY Buffalo report, 1972 (unpublished); M. J. Potoczak, SUNY Buffalo report, 1972 (unpublished).

[12]L. N. Hand, Phys. Rev. 129, 1834 (1963).

[13]T. J. Braunstein, W. L. Lakin, F. Martin, M. L. Perl, W. T. Toner, and T. F. Zipf, Phys. Rev. D 6, 106 (1972).

[14]M.-S. Chen et al., Phys. Rev. Lett. 26, 1585 (1971); M.-S. Chen, L.-L. Wang, and T. F. Wong, ibid. 26, 280 (1971); R. W. Anthony et al., ibid. 26, 38 (1971); N. N. Biswas et al., ibid. 26, 1589 (1971); W. Ko and R. L. Lander, ibid. 26, 1064 (1971); N. F. Bali et al., ibid. 25, 557 (1970); H. Bøggild, K. H. Hansen, and M. Suk, Nucl. Phys. B27, 1 (1971).

[15]P. L. Jain and Z. Ahmad, Phys. Rev. Lett. 28, 459 (1972).

[16]W. P. Swanson, M. Davier, I. Derado, D. C. Fries, F. F. Liu, R. F. Mozley, A. C. Odian, J. Park, F. Villa, and D. E. Yount, Phys. Rev. Lett. 27, 1472 (1971).

[17]K. C. Moffeit, J. Ballam, G. B. Chadwick, M. Della-Negra, R. Gearhart, J. J. Murray, P. Seyboth, C. K. Sinclair, I. O. Skillicorn, H. Spitzer, G. Wolf, H. H. Bingham, W. B. Fretter, W. J. Podolsky, M. S. Rabin, A. H. Rosenfeld, R. Windmolders, G. P. Yost, and R. H. Milburn, Phys. Rev. D 5, 1603 (1972).

[18]P. L. Jain and N. J. Wixon, Phys. Rev. Lett. 23, 715 (1969); P. L. Jain, N. J. Wixon, D. A. Phillips, and J. T. Fecteau, Phys. Rev. D 3, 813 (1970).

[19]P. L. Jain and Angela Stern, Phys. Rev. Lett. 26, 980 (1971).

[20]P. L. Jain, R. D. Malucci, and M. J. Potoczak, Phys. Rev. Lett. 24, 526 (1970); 24, 530 (1970); 24, 1467 (1970); Nuovo Cimento Lett. 3, 684 (1970).

[21]W. H. Barkas, Nuclear Research Emulsions (Academic, New York, 1963), p. 264.

[22]C. F. Powell, P. Fowler, and D. Perkins, The Study of Elementary Particles by the Photographic Method (Pergamon, New York, 1960), p. 464.

[23]E. H. Bellamy, Prog. Nucl. Phys. 8, 239 (1966).

[24]A. M. Boyarski et al., SLAC Report No. SLAC-PUB-671, 1969 (unpublished).

[25]P. L. Jain and P. J. McNulty, Phys. Rev. Lett. 14, 611 (1965); P. J. McNulty and P. L. Jain, Phys. Rev. 183, 1160 (1969).

[26]P. L. Jain, SUNY-Buffalo data at 3, 5, 8 GeV/c muon (unpublished).

[27]R. Hagedorn, Nuovo Cimento Suppl. 3, 147 (1965); Nucl. Phys. B24, 93 (1970).

[28]P. L. Jain, SUNY Buffalo data (unpublished).

[29]D. O. Caldwell, V. B. Elings, W. P. Hesse, G. E.

Jahn, R. J. Morrison, F. V. Murphy, and D. E. Yount, Phys. Rev. Lett. 23, 1256 (1969); 25, 609 (1970).

[30]H. Satz and D. Schildknecht, Phys. Lett. 36B, 85 (1971).

[31]P. L. Jain, SUNY Buffalo report (unpublished).

[32]P. L. Jain, Z. Ahmad, R. D. Malucci, M. J. Potoczak, and B. Girard, Nuovo Cimento Lett. 4, 601 (1972).

[33]K. Fujikawa, Phys. Rev. D 4, 2794 (1971).

[34]A functional form for $\sigma_{ph}(K)$ is found by using the data on Cone et al. (Ref. 35) to facilitate the integration of Eq. (11). The integration over E' is performed (via CDC 6400 computer) by using the method of Gaussian quadrature (GQ). Special attention is given to the variable limits which result from the introduction of K as a variable. We then integrate over each angular interval, again using GQ. The integral cross section versus q^2 is obtained by first changing variables in Eq. (11) $(\Omega \rightarrow q^2)$ and integrating (via GQ) from q^2 to q_{max}^2. The integral is found not to be sensitive to the value of q_{max}.

[35]A. A. Cone, K. W. Chen, J. R. Dunning, Jr., G. Hartwig, N. F. Ramsey, J. K. Walker, and R. Wilson, Phys. Rev. 156, 1490 (1967).

[36]C. M. Hoffman, A. D. Liberman, E. Engles, Jr., D. C. Imrie, P. G. Innocenti, R. Wilson, C. Zajde, W. A. Blanpied, D. G. Stairs, and D. Drickey, Phys. Rev. Lett. 22, 659 (1969).

[37]J. D. Bjorken and E. A. Paschos, Phys. Rev. 185, 1975 (1969).

[38]S. D. Drell, D. J. Levy and T.-M. Yan, Phys. Rev. Lett. 22, 744 (1969).

[39]E. A. Paschos, in High Energy Physics, edited by K. T. Mahanthappa, W. D. Walker, and W. E. Brittin (Colorado Associated Univ. Press, Boulder, 1970), p. 125.

[40]H. Moreno and J. Pestieau, Phys. Rev. D 5, 1210 (1972).

[41]P. V. Landshoff and J. C. Polkinghorne, Nucl. Phys. B28, 240 (1971).

[42]V. Rittenberg and H. R. Rubinstein, Phys. Lett. 35B, 50 (1971).

[43]J. J. Sakurai and D. Schildknecht, Phys. Lett. 40B, 121 (1972).

[44]M. Breidenbach and J. Kuti, MIT report, 1972 (unpublished).

[45]C. W. Gardiner and D. P. Majumdar, Phys. Rev. D 2, 151 (1970); 2, 2040 (1970).

[46]S. J Brodsky, F. E. Close, and J. F. Gunion, Phys. Rev. D 5, 1384 (1972).

[47]S. J. Brodsky and J. Pumplin, Phys. Rev. 182, 1994 (1969); K. Gottfried and D. R. Yennie, ibid. 182, 1595 (1969).

[48]W. T. Meyer et al., Phys. Rev. Lett. 28, 1344 (1972).

Four-Pion Decay of the f^0 Meson*

W. M. Bugg, G. T. Condo, and E. L. Hart

University of Tennessee, Knoxville, Tennessee 37916

H. O. Cohn and R. D. McCulloch

Oak Ridge National Laboratory, Oak Ridge, Tennessee 37830

R. J. Endorf, C. P. Horne,† and M. M. Nussbaum

University of Cincinnati, Cincinnati, Ohio 45221

(Received 15 November 1972)

A search for the $\pi^+\pi^+\pi^-\pi^-$ decay mode of the $f^0(1260)$ has been made in 7.87-GeV/c π^+d interactions. We find no evidence for this decay. The ratio of this decay mode relative to the dipion decay mode of the f^0 is consistent with zero and less than 3.3 % with 90% confidence.

There have recently been several reports of a small but statistically significant 4π decay mode of the f^0. Ascoli et al.,[1] obtained a corrected ratio for $F = f^0 \rightarrow \pi^+\pi^+\pi^-\pi^-/f^0 \rightarrow \pi\pi$ of $(7 \pm 4)\%$ from a 5.1-GeV/c π^-p experiment, while Oh et al.,[2] reported the ratio to be $(7 \pm 2)\%$ from a 7-GeV/c π^-p experiment. On the other hand, the most recent results by Bardadin-Otwinowska et al.,[3] from a study of 8-GeV/c π^+p interactions, show little evidence for the four-pion decay of the f^0. They obtain a ratio $F = (2.2 ^{+4.5}_{-2.2})\%$, consistent with zero. The Meson Spectroscopy Table of the Particle

Data Group[4] gives a world average of $F = (6.1 \pm 1.5)\%$. Our data, presented below, are in agreement with a null result.

The results are obtained from a 0.6-μb event exposure of the BNL 80-in. deuterium bubble chamber exposed to a beam of 7.87-GeV/c π^+ mesons. Only events with a spectator proton identifiable on the scanning table have been selected. The channels relevant to the present work are

(a) $\pi^+d \rightarrow p_s p \pi^+\pi^-$ $(-t \leqslant 10m_\pi^2)$ (963 events),

(b) $\pi^+d \rightarrow p_s p \pi^+\pi^-\pi^+\pi^-$ $(-t \leqslant 10m_\pi^2)$ (92 events),